Non-Cooperative Full-Envelope Calibration of a Supersonic Air Data System

Juan D. Jurado
Electrical and Computer Engineering
U.S. Air Force Academy
Colorado Springs, USA
0000-0003-3600-6239

Clark C. McGehee
School of Advanced Air and Space Studies
Air University
Maxwell AFB, USA
0009-0007-6650-3427

***Abstract*—Air Data Systems require accurate calibration to compensate for errors caused by the disturbed flow field over their pressure ports. If uncorrected, these pressure errors lead to errors in the aircraft's airspeed and altitude measurements, posing a hazard to flight. This paper proposes a novel calibration method that substantially reduces the flight time required to calibrate an aircraft's air data system by increasing analytical rigor. Traditional altitude and GPS-based calibration methods require minimal post-flight analysis, instead requiring numerous in-flight experiments to determine the system calibration. More recent dynamic calibration methods reduce the required number of dedicated in-flight experiments but still require the test aircraft to fly tightly scripted profiles to satisfy their analytical assumptions. This paper eliminates the requirement for scripted in-flight profiles by combining machine learning methods such as Gaussian Process Regression with an Extended Kalman Filter to produce a full-envelope Air Data System calibration. The proposed algorithm is validated using real-world T-38C flight test data and compared against existing calibration methods.**

***Index Terms*—aircraft, air data computer, sensor calibration, non-cooperative**

I. Introduction

Aircraft are typically equipped with a Pitot-static instrumentation system, sometimes called an Air Data System (ADS). The ADS comprises a Pitot tube, which measures total air pressure (P_T), a static port, which measures static air pressure (P_s), and an Air Data Computer (ADC), which uses Pitot-static formulae to compute airspeed and altitude from total and static pressures. Since both airspeed and altitude are directly derived from pressure, they are intrinsically linked to lift and drag, which in turn, are linked to key aircraft performance parameters such as rotation speed, approach speed, climb rate, specific range, and endurance. The act of flying through an air mass disturbs the flow around the air vehicle. This inherently corrupts the static port's ability to measure ambient pressure (the true atmospheric pressure) and creates an error called Static Position Error (SPE) [1].

SPE, denoted ΔP_p, is defined as the difference between measured static pressure, P_s, and true atmospheric pressure, P_a. For ease of analysis, it is typically normalized by P_s when comparing readings from various flight conditions, as

$$\frac{\Delta P_p}{P_s} = \frac{P_s - P_a}{P_s} \tag{1}$$

Since SPE biases static pressure readings, it yields errors in both airspeed and altitude. SPE is primarily a function of the aircraft's shape, in that the disturbed flow around the aircraft results in the erroneous static pressure measurement. This fact makes it difficult or impossible to determine SPE *a priori*, which drives the requirement for in-flight experiments. However, for a given aircraft configuration and flight condition, SPE is consistent. When considering the full envelope of flight conditions for a particular aircraft, we often assume that SPE is a function Mach number and Angle of Attack (AoA) [2].

Many altitude and GPS-based algorithms leverage this assumption to construct point estimates of SPE as a function of Mach number and AoA [1] [2] [3] [4] [5] [6]. Because of their simplifying assumptions, these techniques require multiple experiments with dedicated or cooperative maneuvering from the test aircraft to solve for each point estimate SPE over the aircraft's Mach and AoA envelope. After all SPE estimates are collected, an analyst can fit a curve that describes SPE as a function of instrument-corrected Mach number (M_{ic}) and AoA. By relaxing some of the simplifying assumptions, newer dynamic maneuvering methods such as [7] can estimate SPE across the entire Mach envelope with a single experiment, resulting in considerable efficiency gains. However, these methods still require cooperative maneuvering or dedicated Flight Test Techniques (FTTs) from the target aircraft to satisfy their remaining assumptions.

This paper proposes a novel algorithm for determining SPE that eliminates the requirement for cooperative aircraft maneuvering. By doing so, it allows for calibration of its ADS during conventional flight profiles and greatly reduces or eliminates the requirement for dedicated air data test events. This is particularly appealing for vehicles with limited maneuvering ability or high operational costs, such as gliders or commercial space flight air vehicles. The proposed algorithm combines the use of an Extended Kalman Filter (EKF) for GPS and pressure sensor fusion, with measurement updates

from multiple atmospheric weather balloons generated by a Gaussian Process Regression (GPR) model.

II. Background

In surveying the air data calibration literature, three classes of techniques are predominant: altitude methods, airspeed methods, and pressure methods. Altitude and airspeed methods seek to determine airspeed and altitude error as a function of Mach number by using external truth sources, such as a calibrated chase aircraft or GPS. In general, these methods are simple to execute and require minimal instrumentation and data analysis. Pressure methods tend to require more instrumentation, but offer the benefit of measuring the static pressure errors directly by comparing the aircraft's static pressure measurement to an offboard truth source like a weather balloon or a trailing cone.

A. Altitude Methods

The most widely used altitude method for SPE calibration is the Tower Fly-by (TFB) [1] [2]. A general TFB diagram is shown in Figure 1. The TFB technique is simple to fly and requires minimal data analysis. The TFB aims to determine an altitude error correction, ΔH_{pc}, by comparing the indicated altitude in the aircraft's altimeter, H_{ic}, to an externally measured reference altitude, H_c, which is derived from a theodolite measurement at a ground-based observation tower. The aircraft flies at a constant altitude and airspeed as it passes by the observation tower, where an observer records the "truth" altitude, H_c. The aircraft records its altitude, H_{ic}, simultaneously. The error correction relationship is given by

$$\Delta H_{pc} = H_c - H_{ic} \tag{2}$$

By repeating this procedure at a range of airspeeds (i.e., Mach numbers), one can construct a curve of altitude errors as a function of Mach number. Since altitude is a function of pressure, one can construct a curve of SPE as a function of Mach by mapping the altitudes to pressures. The SPE curve can then be used to correct the aircraft's static pressure measurements and, thus, its airspeed and altitude measurements. While the TFB is simple and accurate, it requires multiple fly-bys to sample the underlying $\Delta P_p(M_{ic})$ curve, a team of individuals at the tower site to perform manual theodolite readings, and most importantly, a well-surveyed TFB site. Additionally, obtaining TFB data for transonic and supersonic conditions is difficult due to sonic boom concerns for nearby structures and personnel, as well as structural concerns for the test aircraft due to the high dynamic pressure experienced at low-altitude supersonic speeds.

B. Airspeed Methods

Following a similar logic, airspeed methods seek to determine SPE by first determining airspeed error. These methods have seen the most innovation in recent literature due to the emergence and proliferation of Differential Global Positioning System (DGPS) in military and commercial aircraft. The "wind triangle" forms the basis of most airspeed techniques [3]

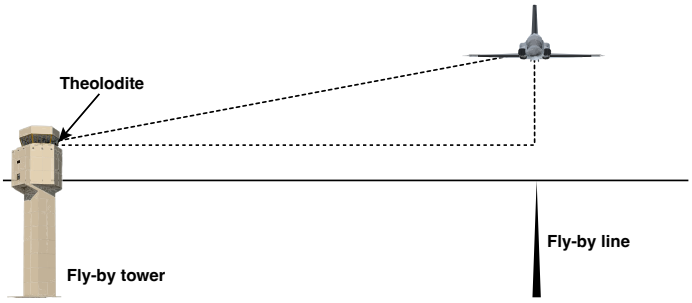

Fig. 1. Illustration of the Tower Fly-by.

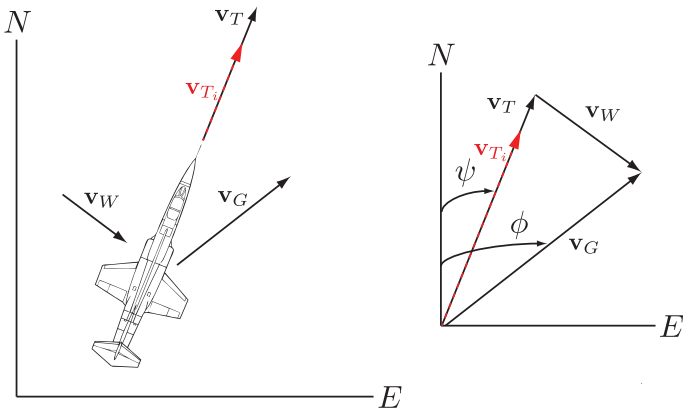

Fig. 2. Illustration of the wind triangle.

[4] [5] [6]. Figure 2 illustrates this simplified two-dimensional transformation from the body frame (*b*-frame) to the navigation frame (*n*-frame).

In [4], the true airspeed error, ΔV_T, which is caused by SPE, is estimated using DGPS by assuming a constant and unknown wind vector. The aircraft flies a 360-degree turn at a constant indicated altitude and indicated airspeed, which allows the unknown parameters ($\mathbf{v}_W$ and $\mathbf{v}_{T_i}$) to become observable to a linear model. The model is developed using two-dimensional vector geometry from the wind triangle using

$$\Delta V_T \cos(\psi) + v_{W_N} = v_G \cos(\phi) - v_{T_i} \cos(\psi) \tag{3}$$
$$\Delta V_T \sin(\psi) + v_{W_E} = v_G \sin(\phi) - v_{T_i} \sin(\psi) \tag{4}$$

where v_{T_i} is the aircraft's measured (or SPE corrupted) True Airspeed (TAS), ψ is true heading, v_G and ϕ are ground speed and ground track respectively, as measured by DGPS, ΔV_T is the unknown TAS error, and v_{W_N} and v_{W_E} are the unknown constant wind vector components. Having obtained ΔV_T, the airspeed error can be converted to a pressure error, ΔP_p for the specific Mach number flown [2], with the assumption that there is no total pressure P_T error in the system. Much like the TFB, this method requires multiple experiments to collect point estimates of the underlying $\Delta V_{pc}(M_{ic})$ function across the full Mach range. It also requires cooperative maneuvering (e.g., executing a level turn at a constant Mach number) by the target aircraft. Additionally, the estimation process is non-trivial: v_{T_i} is difficult to measure since it must be derived

from Indicated Airspeed (IAS), V_{ic}, and ambient temperature, T_a, which itself requires external calibration from the TFB or weather balloons.

To overcome some of these challenges, another class of calibration methods [6] [7] [8] [9] [10], use recursive estimation techniques such as the Kalman Filter (KF) [11] to converge onto calibration parameters of interest. Notably, in [7], the underlying SPE curve is estimated as a function of Mach number using as little as a single experiment or test point, using a Backwards Smoothing Extended Kalman Filter (BSEKF) [12] and a cooperative FTT consisting of a level acceleration, which allows for characterization of the Mach number dependency, and a level turn, which allows for estimation of the unknown wind vector. While these methods increase efficiency by relaxing the aforementioned assumptions, they still require dedicated and cooperative aircraft maneuvering to converge on a reliable estimate of SPE.

C. External Reference Methods

One of the most accurate methods for estimating SPE is the pressure survey method [1]. In this technique, a weather balloon capable of measuring P_a, T_a, and GPS altitude, H_g, is launched into the local airmass. The balloon measurements of P_a can then directly be used to compute SPE using (1). This method provides the most accurate results since it directly measures the desired error. The survey method is limited by the assumed constant atmospheric properties between the balloon launch site and the area where the experimental aircraft collects its data. This assumption also limits the ability to perform this technique online since the truth data needed for calibration is only available and/or valid for a limited time and geographical region.

D. Contributions

Having explored the underlying characteristics of the SPE problem and the state-of-the-art solutions, we now turn to the proposed algorithm, henceforth referred to as Non-Cooperative Calibration for Air Data Systems (NCADS), and its specific contributions. The proposed NCADS algorithm:

(a) Builds on the hybrid pressure-airspeed-altitude algorithm from [7] by eliminating the need for cooperative aircraft maneuvering.
(b) Enables full Mach number domain characterization including transonic and supersonic effects using a single experiment.
(c) Optimally combines multiple external weather balloon measurements into a GPR model to create an atmospheric sensor model for a BSEKF.

E. Outline

The remainder of this paper is organized into three additional sections. Section III develops the flying and data processing algorithms that enable the research advancements proposed herein. Section IV presents results from a T-38C flight test program comparing the proposed algorithm against state-of-the-art methods. Finally, Section V summarizes the research effort, and presents conclusions and future work.

III. Methodology

A. General Approach

The general approach of the NCADS algorithm contains four steps:

(a) Create an atmospheric sensor model for use in a BSEKF by combining readings from any number of weather balloons into a single GPR model.
(b) Create a GPS velocity sensor model for use in a BSEKF by equating the relationship between 3D GPS velocity, aircraft attitude, static pressure, and ambient temperature.
(c) Use the above sensor models in a five-state BSEKF to produce optimal estimates of ambient pressure, ambient temperature, and three-dimensional wind.
(d) Use the estimated ambient pressure readings from the BSEKF and (1) to produce estimates of SPE, then fit a smoothing spline model through the resulting SPE observations to produce a final lookup table for the ADC.

B. BSEKF State Dynamics

The NCADS algorithm uses a five-state BSEKF to produce estimates of the state vector

$$\mathbf{x}_k = \left[\ P_a(t_k), T_a(t_k), v_{W_N}(t_k), v_{W_E}(t_k), v_{W_D}(t_k)\ \right]^\top \quad (5)$$

where t_k is the time at sample k, P_a is ambient pressure, T_a is ambient temperature, and $v_{W_N}, v_{W_E}, v_{W_D}$, are the North, East, and Down wind velocities, respectively.

The propagation dynamics for the pressure (P_a) and temperature (T_a) states are computed using the standard atmosphere [13] equations and based on the change in GPS altitude (H_g) between t_k and t_{k+1} using:

$$P_a(t_{k+1}) = P_a(t_k) + \Delta P_a \quad (6)$$
$$\Delta P_a = P_{SL}\left(\delta\left[H_g(t_k)\right] - \delta\left[H_g(t_{k+1})\right]\right) \quad (7)$$
$$T_a(t_{k+1}) = T_a(t_k) + \Delta T_a \quad (8)$$
$$\Delta T_a = T_{SL}\left(\theta\left[H_g(t_k)\right] - \theta\left[H_g(t_{k+1})\right]\right) \quad (9)$$

where δ is the pressure ratio function, P_{SL} is sea-level pressure, θ is the temperature ratio function, and T_{SL} is sea-level temperature, as defined in the standard atmosphere model [2] [13].

Since both the pressure ratio (δ) and temperature ratio (θ) functions are sampled using GPS altitude (H_g) instead of the unknown true pressure altitude (H_c), the BSEKF discrete-time propagation noise uncertainty matrix ($\mathbf{Q}_d$) for both P_a and T_a states is constructed using:

$$\mathbf{Q}_{d_{P_a}} = \sigma^2_{P_a}\Delta P_a \quad (10)$$
$$\mathbf{Q}_{d_{T_a}} = \sigma^2_{T_a}\Delta T_a \quad (11)$$

where the variances $\sigma^2_{P_a}$ and $\sigma^2_{T_a}$ are the appropriately tuned to allow for subsequent measurement updates to effectively

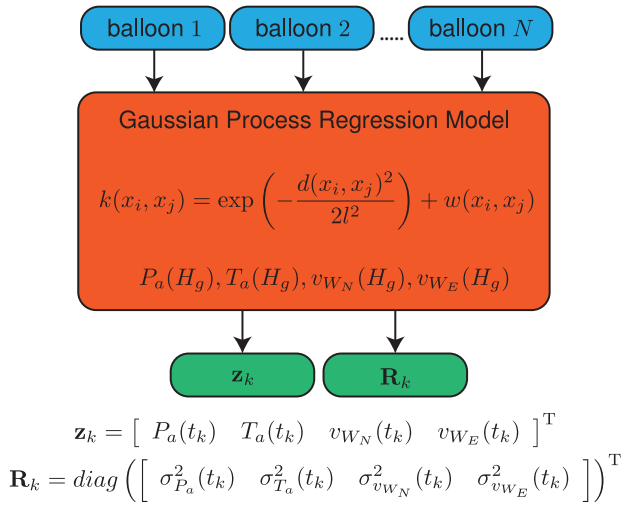

Fig. 3. Illustration of GPR atmospheric model for BSEKF.

correct the state estimates. For the results presented in this paper, the variances were set as follows:

$$\sigma^2_{P_a} = 2^2 \text{ [psi}^2\text{]} \tag{12}$$
$$\sigma^2_{T_a} = 2^2 \text{ [K}^2\text{]} \tag{13}$$

The propagation dynamics for the North, East, and Down wind ($v_{W_N}, v_{W_E}, v_{W_D}$) states were modeled as a three-state First Order Gauss-Markov (FOGM) process [14] using GPS altitude (H_g) as the correlation variable. For the results presented in this paper, the FOGM parameters were set as:

$$\sigma_{V_w} = \begin{bmatrix} 30 & 30 & 1 \end{bmatrix} \text{ [kts]} \tag{14}$$
$$\tau_{V_w} = \begin{bmatrix} 100 & 100 & 1 \end{bmatrix} \text{ [ft]} \tag{15}$$

where each of the three dimensions in the vectors in (14) and (15) correspond to the North, East, and Down wind state components.

C. Atmospheric Sensor Model

Having established state propagation dynamics for the five BSEKF states, we now turn to the first measurement model used to correct state estimates using sensor updates. As illustrated in Section II-C, one of the main disadvantages of external reference methods for ADS calibration was the limited accuracy of using a single weather balloon to model the entire geographical area used during the flight profile. Here we introduce the use of machine learning methods such as GPR [15] to not only produce fused Pa, T_a, v_{W_N}, and v_{W_E} measurements from multiple weather balloons, but also estimate the variance in such measurements so they can be effectively integrated into the BSEKF. Using notation from [16], BSEKF measurement updates are computed using:

$$\mathbf{r}_k = \mathbf{z}_k - \mathbf{H}_k \hat{\mathbf{x}}_k^- \tag{16}$$
$$\mathbf{K}_k = \mathbf{P}_k^- \mathbf{H}_k^{\mathrm{T}} \left(\mathbf{H}_k \mathbf{P}_k^- \mathbf{H}_k^{\mathrm{T}} + \mathbf{R}_k\right)^{-1} \tag{17}$$
$$\hat{\mathbf{x}}_k^+ = \hat{\mathbf{x}}_k^- + \mathbf{K}_k \mathbf{r}_k \tag{18}$$
$$\mathbf{P}_k^+ = \mathbf{P}_k^- - \mathbf{K}_k \mathbf{H}_k \mathbf{P}_k^- \tag{19}$$

where $\mathbf{z}_k$ is the measurement vector at time t_k, $\mathbf{H}_k$ is the measurement matrix (or linearized measurement function for nonlinear measurements), $\mathbf{R}_k$ is the measurement noise covariance matrix, $\hat{\mathbf{x}}_k^-$ and $\hat{\mathbf{x}}_k^+$ are the pre- and post-update state estimates, and $\mathbf{P}_k^-$ and $\mathbf{P}_k^+$ are the pre- and post-update state estimation covariance matrices, respectively. As shown in (16)-(19), expressing weather balloon measurements using $\mathbf{z}_k$ and $\mathbf{R}_k$ is required to integrate them into the BSEKF.

In general, a GPR model [15] can be considered a type of machine learning process, and it is useful where the observations being modeled do not fit the assumptions of a linear model [17] or the form of their relationship is not well known *a priori*. Unlike a linear model of the form

$$\mathbf{y} = \mathbf{X}\boldsymbol{\beta} + \boldsymbol{\epsilon} \tag{20}$$

where $\mathbf{y}$ is the vector of observations, $\mathbf{X}$ is the linear model design matrix, and $\boldsymbol{\epsilon}$ is a vector of Independent Identically Distributed (IID) White Gaussian Noise (WGN), a GPR model follows the form

$$P(\mathbf{y}|\mathbf{X}) = \mathcal{N}(\mathbf{y}|\boldsymbol{\mu}, \mathbf{K}) \tag{21}$$

where $\boldsymbol{\mu}$ is the vector of mean values for the chosen kernel function, and $\mathbf{K}$ is the kernel's covariance function. For the results presented in this research, the following kernel covariance functions were used

$$k(x_i, x_j) = \exp\left(-\frac{d(x_i, x_j)^2}{2l^2}\right) + w(x_i, x_j) \tag{22}$$

where $d(x_i, x_j)$ is the Euclidean distance between x_i and x_j, l is the length scale of the kernel (set to a value of 1 for the results shown), and w is given by

$$w(x_i, x_j) = \begin{cases} \sigma^2, & \text{if } i = j \\ 0, & i \neq j \end{cases} \tag{23}$$

where σ^2 is the noise level parameter of the kernel (set to a value of 1 for the results shown). For this research, a four-dimensional BSEKF measurement model was formed by fitting a separate GPR model for $\mathbf{y} = P_a$, T_a, v_{W_N} and v_{W_E}, each as a function of GPS altitude, i.e. $\mathbf{X}_k = H_g(t_k)$. Figure 3 illustrates the process of producing a single four-dimensional measurement model from any number of N independent weather balloons.

D. GPS Velocity Sensor Model

Given the potential geographical distance between the aircraft and the area where the weather balloons sampled the atmosphere, as well as the possibility of the aircraft exceeding the GPS altitude envelope of the weather balloons, it is also important to consider the onboard GPS velocity information as a means to improve the estimates of the BSEKF states. The NCADS algorithm uses a modified version of the GPS measurement update developed in [7]. In general, we consider the wind triangle illustrated in Figure 2 but using its three-dimensional form including roll, pitch, yaw, AoA, and Angle of Sideslip (AoS) angles, to relate measured GPS velocities to

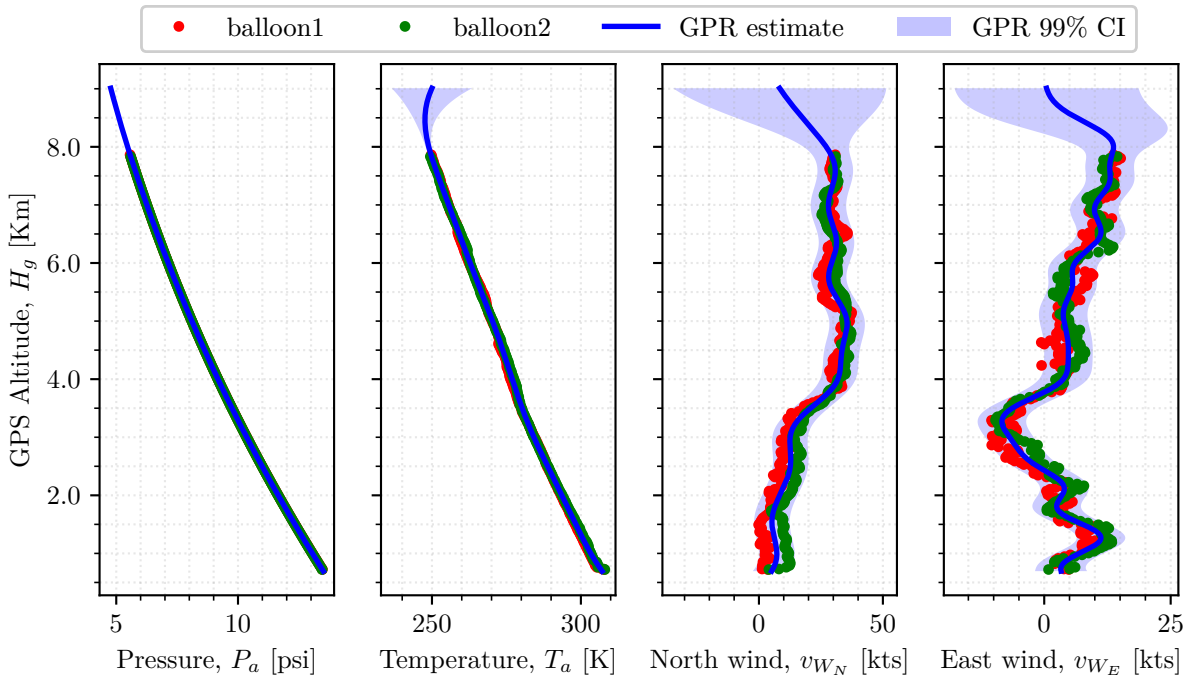

Fig. 4. Example GPR model using measurements from two weather balloons.

the aircraft's TAS. The GPS velocity measurement model in NCADS is developed using

$$\hat{M}_{pc} = f(\hat{P}_a, P_T) \tag{24}$$

$$\hat{a} = a_{SL}\sqrt{\frac{\hat{T}_a}{T_{SL}}} \tag{25}$$

$$\hat{v}_T = \hat{M}_{pc}\hat{a} \tag{26}$$

$$\hat{\mathbf{v}}_T^w = \begin{bmatrix} \hat{v}_T & 0 & 0 \end{bmatrix}^{\mathrm{T}} \tag{27}$$

$$\hat{\mathbf{v}}_T^n = \mathbf{C}_b^n \mathbf{C}_w^b \hat{\mathbf{v}}_T^w \tag{28}$$

$$\hat{\mathbf{v}}_g^n = \hat{\mathbf{v}}_T^n + \begin{bmatrix} \hat{v}_{W_N} & \hat{v}_{W_E} & \hat{v}_{W_D} \end{bmatrix}^{\mathrm{T}} \tag{29}$$

where the function in (24) is given in [2], the Direction Cosine Matrices (DCMs) $\mathbf{C}_b^n$, and $\mathbf{C}_w^b$ are created using the rotation matrices defined in [18], and $\hat{\mathbf{v}}_g^n$ is the estimated GPS velocity vector to be used in the BSEKF measurement update.

E. Final SPE Model

Leveraging the use of NCADS in its ability to omit dedicated or cooperative experiments for calibration, a single flight sortie from takeoff to landing can be processed through the BSEKF to produce a time history of estimated variables. Given BSEKF estimates of P_a, estimated SPE observations can then be computed using (1). Next, given a time history of SPE and corresponding M_{ic}, we use a smoothing spline model [19] to compute the final SPE vs. M_{ic} lookup table for the aircraft's ADC. For the results presented in this paper, the following smoothing spline "knot" locations ($\mathbf{k}$) were used:

$$\mathbf{k} = \begin{bmatrix} 0 & 0.8 & 0.9 & 0.95 & 0.96 & 0.97 & 1.02 \end{bmatrix} \tag{30}$$

IV. Results

Figure 4 illustrates the results of P_a, T_a, v_{W_N} and v_{W_E} GPR models generated using observations from two independent weather balloons. As shown, the GPR model effectively produced estimates of the appropriate atmospheric parameters along with estimated model covariance to be used in the BSEKF. It is important to note the appropriate growth in model covariance as the sampled altitude exceeds the upper limit of the balloon observations. A single T-38C flight lasting approximately 1.1 hours was processed entirely from takeoff to landing with the NCADS algorithm, using measurement updates from onboard GPS velocities, and the atmospheric GPR model from the two weather balloons. Figure 5 illustrates the BSEKF-derived SPE observations in blue plotted against M_{ic} along with the final smoothing spline model in red. Finally, the existing T-38C SPE lookup table is plotted in green for comparison. The existing lookup table was derived using data from existing GPS and external reference methods spanning approximately 6.6 flight hours and multiple dedicated experiments. Note the installed SPE model does not cover the M_{ic} range between 0 and 0.3 due to the limitations of the necessary in-flight cooperative maneuvers. As shown, the NCADS algorithm was able to effectively reproduce the

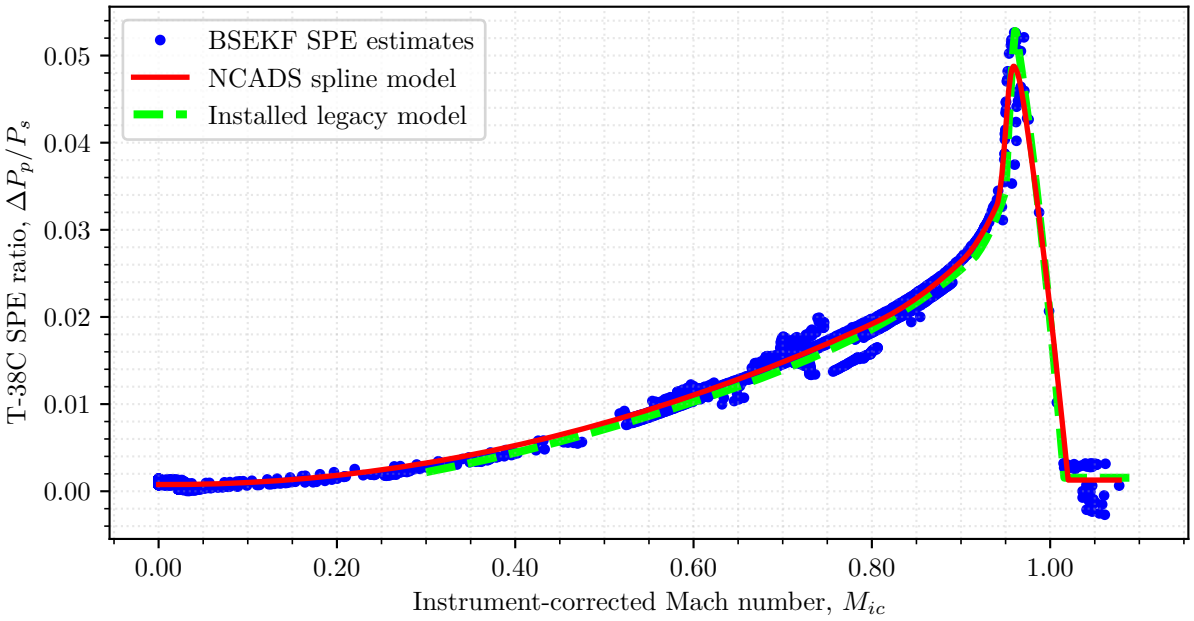

Fig. 5. SPE model for T-38C derived using NCADS algorithm over a single flight.

existing SPE model for the target aircraft using a single flight with no dedicated experiments or FTTs, and produced a curve spanning the entire M_{ic} envelope from 0.0 to 1.02.

V. Conclusions

This paper has developed a novel algorithm for aircraft ADS calibration capable of producing full-envelope results using a single flight, without the need for dedicated experiments or FTTs. The algorithm was validated using real-world data from a T-38C flight test experiment and compared against existing methods. As demonstrated, the NCADS algorithm effectively reduces flight test time needed for ADS calibration for all aircraft, and is especially suitable for aircraft where dedicated experiments are infeasible or impractical, such as non-powered aircraft and commercial space air vehicles.

References

[1] E. A. Haering Jr, "Airdata measurement and calibration," NASA, Technical Memorandum 104316, 1995.

[2] R. E. Erb, *Pitot-statics Textbook*, 4th ed. USAF Test Pilot School, 2020.

[3] G. V. Lewis, "A flight test technique using gps for position error correction testing," in *COCKPIT, Society of Experimental Test Pilots Quaterly Publication*, March 1997.

[4] T. R. Jorris, M. M. Ramos, R. E. Erb, and R. K. Woolf, "Statistical pitot-static calibration technique using turns and self-survey method," in *42nd International SFTE Symposium*, Seattle, Washington, August 2011.

[5] W. M. Olson, "Pitot-static calibrations using a gps multi-track method," in *28th SFTE Symposium*, September 1998.

[6] R. J. Niewoehner, "Refining satellite methods for pitot-static calibration," *Journal of Aircraft*, vol. 43, no. 3, pp. 846–849, may 2006. [Online]. Available: https://doi.org/10.2514%2F1.18976

[7] J. D. Jurado and C. C. McGehee, "Complete online algorithm for air data system calibration," *Journal of Aircraft*, vol. 56, no. 2, pp. 517–528, 2019.

[8] A. Cho, Y.-s. Kang, B.-j. Park, C.-s. Yoo, and S.-o. Koo, "Air data System Calibration Using GPS Velocity information," *2012 International Conference on Control, Automation and Systems International Conference on Control, Automation and Systems*, pp. 433–436, 2012.

[9] T. A. Johansen, A. Cristofaro, K. Sorensen, J. M. Hansen, and T. I. Fossen, "On estimation of wind velocity, angle-of-attack and sideslip angle of small UAVs using standard sensors," in *2015 International Conference on Unmanned Aircraft Systems (ICUAS)*. IEEE, jun 2015. [Online]. Available: https://doi.org/10.1109%2Ficuas.2015.7152330

[10] E. A. Haering Jr, "Airdata calibration techniques for measuring atmospheric wind profiles," *Journal of Aircraft*, vol. 29, no. 4, pp. 632–639, jul 1992. [Online]. Available: https://doi.org/10.2514%2F3.46212

[11] R. E. Kalman, "A new approach to linear filtering and prediction problems," *Journal of Basic Engineering*, vol. 82, no. 1, p. 35, 1960. [Online]. Available: https://doi.org/10.1115%2F1.3662552

[12] M. L. Psiaki, "Backward-smoothing extended kalman filter," *Journal of Guidance, Control, and Dynamics*, vol. 28, no. 5, pp. 885–894, sep 2005. [Online]. Available: https://doi.org/10.2514%2F1.12108

[13] U. S. Atmosphere, *US standard atmosphere*. National Oceanic and Atmospheric Administration, 1976.

[14] P. S. Maybeck, *Stochastic Models, Estimation, and Control Volume 1*. Virginia: Navtech, 1982.

[15] C. K. Williams and C. E. Rasmussen, *Gaussian Processes for Machine Learning*. MIT press Cambridge, MA, 2006, vol. 2, no. 3.

[16] P. S. Maybeck, *Stochastic Models, Estimation, and Control Volume 2*. Virginia: Navtech, 1984.

[17] M. H. Kutner, C. Nachtsheim, and J. Neter, *Applied Linear Regression Models*. McGraw-Hill/Irwin, 2004, vol. 4.

[18] T. G. Gainer and S. Hoffman, "Summary of transformation equations and equations of motion used in free flight and wind tunnel data reduction and analysis," NASA, Technical Report NASA-SP-3070, 1972.

[19] D. Ruppert, "Selecting the number of knots for penalized splines," *Journal of computational and graphical statistics*, vol. 11, no. 4, pp. 735–757, 2002.